



Azimuthal anisotropy and mantle flow underneath the southeastern Tibetan Plateau and northern Indochina Peninsula revealed by shear wave splitting analyses

Fansheng Kong^{a,b}, Jing Wu^c, Lin Liu^b, Kelly H. Liu^b, Jianguo Song^d, Jiabiao Li^a, Stephen S. Gao^{b,*}

^a Key Laboratory of Submarine Geosciences, Second Institute of Oceanography, State Oceanic Administration, Hangzhou 310012, China

^b Geology and Geophysics Program, Missouri University of Science and Technology, Rolla, Missouri 65409, USA

^c State Key Laboratory of Lithospheric Evolution, Institute of Geology and Geophysics, Chinese Academy of Sciences, Beijing 100029, China

^d School of Geosciences, China University of Petroleum (East China), Qingdao 266580, China

ARTICLE INFO

Keywords:

Seismic anisotropy
Southeastern Tibetan Plateau
Slab rollback
Shear wave splitting

ABSTRACT

Seismic azimuthal anisotropy beneath the transitional region between the southeastern Tibetan Plateau and the Indochina Peninsula, an area in which the fast orientation of mantle anisotropy changes to dominantly E-W from mostly N-S on the plateau at the north, is quantified using splitting of the SKS, SKKS, and PKS phases. Among the 50 stations with one or more splitting measurements, 22 possess an azimuthal coverage that is adequate for the identification and characterization of complex anisotropy. The resulting splitting parameters from 15 such stations exhibit systematic back azimuthal variations with a 90° periodicity, which is consistent with a two-layered anisotropy model. The upper layer parameters are consistent with crustal anisotropy measurements obtained independently based on the sinusoidal moveout of P-to-S conversions from the Moho, with the fast orientations being mostly parallel to major shear zones. The lower layer fast orientations and the fast orientations at stations with azimuthally invariant splitting parameters are mostly E-W, which is significantly different from the dominantly N-S trend of the surface expression of major structural fabrics in the area. They are also inconsistent with the absolute plate motion directions. When combined with results from seismic tomography and focal mechanism solutions, the observed azimuthal anisotropy can be adequately explained by the movement of the lithosphere relative to the underlain asthenosphere, most likely associated with the westward rollback of the subducted Indian Plate.

1. Introduction

To explain the uplifting and evolution of the Tibetan Plateau, which is generally regarded as the consequence of subduction of the Indian lithosphere beneath the Eurasian Plate, distinct geodynamic models such as tectonic escape (Tapponnier, 1982) and upper or lower crustal thickening (England and Houseman, 1986; Bird, 1991; Royden et al., 1997; Chen et al., 2017) have been proposed over the past several decades (Yin and Harrison, 2000). Another consequence of the continental convergence is the extrusion of crustal and mantle materials from the plateau toward the southeast into adjacent regions (Tapponnier, 1982; Royden et al., 1997; Liu et al., 2004; Gan et al., 2007; Zhang et al., 2010; Searle et al., 2011; Huang et al., 2015a), although this model remains debated (e.g., England and Molnar, 1990). Numerous studies have suggested remarkable influences of the convergence on far-field deformations such as the volcanoes in Hainan and

Vietnam, and the spreading of the South China Sea (e.g., Li et al., 2008; Huang et al., 2015c). The influences are evident from the extensive strike-slip faults and the Global Positioning System (GPS) velocities (Gan et al., 2007), both reflecting the deformation field of the Earth's surface. The deformation field at depth, however, is less understood and can be characterized by shear wave splitting analyses, as detailed below.

The study area (Fig. 1) is the transitional zone between the southeastern Tibetan Plateau and the Indochina Peninsula. It mainly composes of three tectonic provinces (Searle, 2006; Wang et al., 2010), including the Shan-Thai Block of the Indochina Peninsula west of the Red River Fault, the Yangtze Block east of the Xianshuihe-Xiaojiang Fault, and the southernmost region of the Qiangtang Block of the Tibetan Plateau between the two faults. Recent seismic tomography studies reveal a slab-like high velocity zone extending to the mantle transition zone or the upper part of the lower mantle, and interpret it as

* Corresponding author.

E-mail address: sgao@mst.edu (S.S. Gao).

<https://doi.org/10.1016/j.tecto.2018.09.013>

Received 17 May 2018; Received in revised form 19 September 2018; Accepted 21 September 2018

Available online 27 September 2018

0040-1951/ © 2018 Elsevier B.V. All rights reserved.

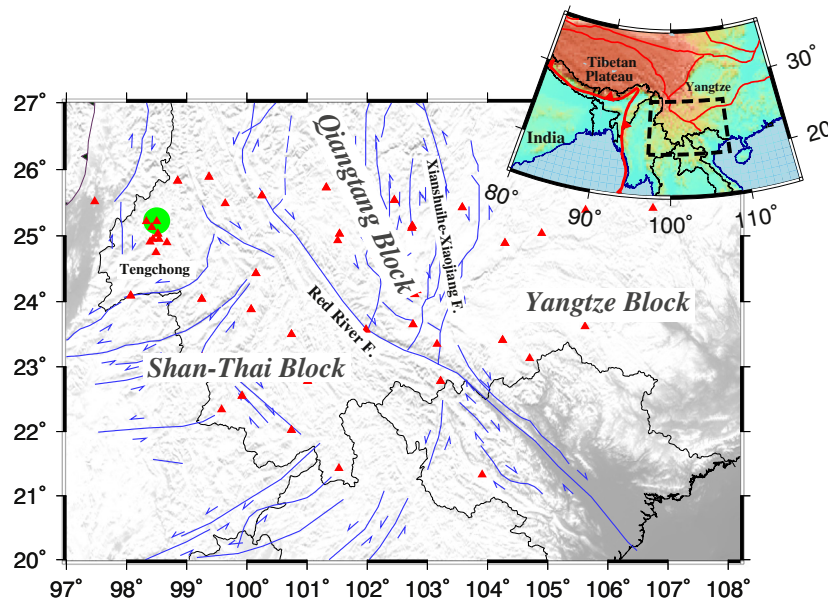


Fig. 1. Map of the study area showing major faults (Styron et al., 2010) and seismic stations (red triangles) used in the study. The green circle indicates the Tengchong volcano. The inset map shows the study area.

the subducted Indian Plate (Li et al., 2008; Wei et al., 2012; Huang et al., 2015a). To the west of the Red River Fault, a large low velocity zone is detected in the upper mantle of the Shan-Thai Block, and is inferred to be a consequence of either the dehydration (Lei et al., 2009; Wei et al., 2012) or mantle processes associated with the westward rollback of the Indian Plate (Li et al., 2008), which is consistent with the absence of thrust faulting mechanisms (Zhao et al., 2013a).

1.1. Simple and complex seismic anisotropy

The mantle deformation and mantle flow fields associated with the subduction and tectonic extrusion can be readily studied by measuring the orientation and magnitude of seismic azimuthal anisotropy (Zhang and Karato, 1995), which is quantified by shear wave splitting (SWS) analysis using teleseismic SKS, SKKS, and PKS waves (collectively called XKS hereafter; Silver and Chan, 1991; Gao et al., 1994, 2010; Wu et al., 2015; Cherie et al., 2016). When a shear wave travels through a transversely isotropic medium which is the simplest form of azimuthal anisotropy, it splits into two shear waves with orthogonal polarization orientations. The splitting parameters, including the polarization orientation of the fast wave (ϕ) and the splitting delay time between the fast and slow waves (δt), convey essential information on the orientation and strength of azimuthal anisotropy, respectively. In the upper mantle, anisotropy is generally regarded as the consequence of lattice preferred orientation of anisotropic minerals, primarily olivine (Zhang and Karato, 1995). For A-type olivine fabric that is the most abundant type in the continental upper mantle (Ben Ismail and Mainprice, 1998), shear strain induced by mantle flow field aligns the a axis of olivine to be parallel to the flow direction. When the lithosphere experiences vertically coherent compression, the resulting ϕ is normal to the maximum compressional stress (Silver and Chan, 1991; Wang et al., 2008).

The vast majority of SWS parameters, including those in the study area (Fig. 2), were measured under the assumption of simple anisotropy, i.e., a single layer of transverse isotropy with a horizontal axis of symmetry. Such an ideal scenario results in individual splitting parameters that are invariant to the arriving azimuth (the back azimuth or BAZ) of the events, and consequently, station-averaged splitting parameters can adequately represent the anisotropic properties. Any significant departure from the characteristics of simple anisotropy leads to complex anisotropy, for which a model consisting of two anisotropic

layers with horizontal axes of symmetry is the most common form (Silver and Savage, 1994). Except for the special situation when the fast orientations of the two layers are parallel or orthogonal to each other, the individual splitting parameters from such a two-layered model show a systematic variation against the BAZ with a 90° periodicity (Silver and Savage, 1994).

The azimuthal dependence of the individual splitting parameter suggests that station-averaged splitting parameters cannot objectively reflect the actual anisotropic properties. Unfortunately, as detailed in Liu and Gao (2013) and demonstrated by Cherie et al. (2016) and other studies, it is usually difficult to reliably judge the existence of complex anisotropy due to the limited BAZ coverage (especially when only the SKS phase is used), frequently leading to controversial conclusions about the geodynamic implications of splitting measurements (e.g., Wang et al., 2008 and Huang et al., 2015b for the SE Tibetan Plateau). Other P-to-S converted phases at the core mantle boundary such as SKKS and PKS are essential to improve the azimuthal coverage, especially for SWS studies in East and Southeast Asia where the majority of the SKS events are from a narrow BAZ band (Fig. 3).

1.2. Previous shear wave splitting measurements and objectives of the present study

To investigate mantle deformation presumably associated with the Indo-Tibetan collision, numerous SWS studies have been conducted on the southeastern Tibetan Plateau and adjacent regions (e.g., Flesch et al., 2005; Chang et al., 2006; Lev et al., 2006; Sol et al., 2007; Wang et al., 2008; Shi et al., 2012; Wang et al., 2013; Zhao et al., 2013b; Huang et al., 2015b). Most of the studies used only SKS events that mainly situated in the western Pacific subduction zones spanning a narrow BAZ range of $\sim 110^\circ$ – 140° (Fig. 3). A few studies included some SKKS events (e.g., Lev et al., 2006; Shi et al., 2012; Huang et al., 2015b), but only used events with an epicentral distance less than 140° and thus excluded the majority of usable SKKS events that were mostly from the western coastal area of South America that is farther than 140° (Fig. 3). Except for a single attempt to quantify complex anisotropy at a few stations with a short recording duration of 13 months (Lev et al., 2006), to our knowledge, no systematic investigations on the azimuthal variations of shear wave splitting parameters for the purpose of identifying and quantifying complex anisotropy have been conducted in the

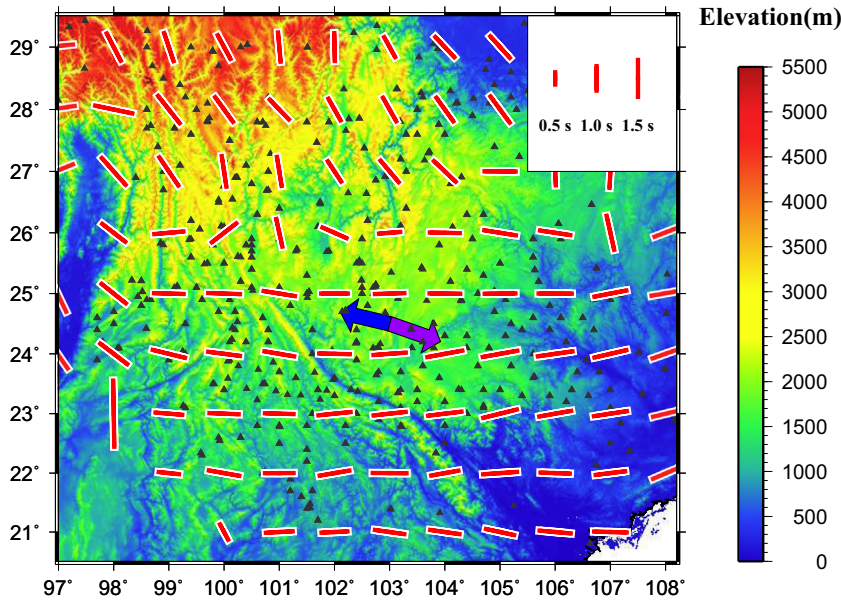


Fig. 2. The red bars show area-averaged (in radius=1° circular bins) previous shear wave splitting measurements (Lev et al., 2006; Sol et al., 2007; Wang et al., 2008; Shi et al., 2012; Wang et al., 2013; Zhao et al., 2013b; Huang et al., 2015b) obtained using the measurements from stations that are located in the bins defined with a radius of 1°. The orientation of the bars represents the fast orientation, and the length is proportional to the delay time (see scale bars in the upper right corner). Purple and blue arrows represent the absolute plate motion from the NNR-MORVEL56 (Argus et al., 2011) and HS3-NUVEL1A (Gripp and Gordon, 2002) models, respectively. The black triangles denote the locations of the stations. In the study area the APM rate is 22–24 mm/yr, and the orientation is 15–20° from the E-W direction for both models.

study area.

The area-averaged splitting parameters from previous studies demonstrate a sudden change of the fast orientations from mostly N-S to dominantly E-W at about ~ 26°N (Fig. 2). The area-averaged splitting parameters are computed by taking the circular (for ϕ) and simple (for δt) means over previous splitting measurements (Lev et al., 2006; Sol et al., 2007; Wang et al., 2008; Shi et al., 2012; Wang et al., 2013; Zhao et al., 2013b; Huang et al., 2015b) at stations within consecutive circular bins with a radius of 1°. The distance between the center of neighboring bins is 1°.

A number of mechanisms for this intriguing observation have been proposed, including the transition of deformation from simple shear in SE Tibetan Plateau to pure shear in adjacent regions (e.g., Wang et al., 2008), lateral variations in lithospheric rheology (e.g., Lev et al., 2006), influences from distant subduction processes (Lev et al., 2006; Huang

et al., 2015b), and different origins of seismic anisotropy with a dominant lithospheric source in the SE Tibetan Plateau and a significant contribution from the asthenosphere in the adjacent regions (Sol et al., 2007; Huang et al., 2015b). In addition, Yao et al. (2010) suggest a significant contribution from crustal anisotropy to the observed XKS splittings on the Plateau, and a mostly upper mantle source off the Plateau.

The assumption of simple anisotropy utilized by most previous studies in the area dominated by E-W fast orientations neglects potentially significant crustal contributions to the observed XKS splitting (Sun et al., 2012). More importantly, it may not objectively reveal dynamic processes that led to the observed anisotropy. In this study, we conduct shear wave splitting analyses beneath the southeastern Tibetan Plateau and adjacent regions to investigate crustal and mantle anisotropic structures using teleseismic SKS, SKKS, and PKS phases, as well

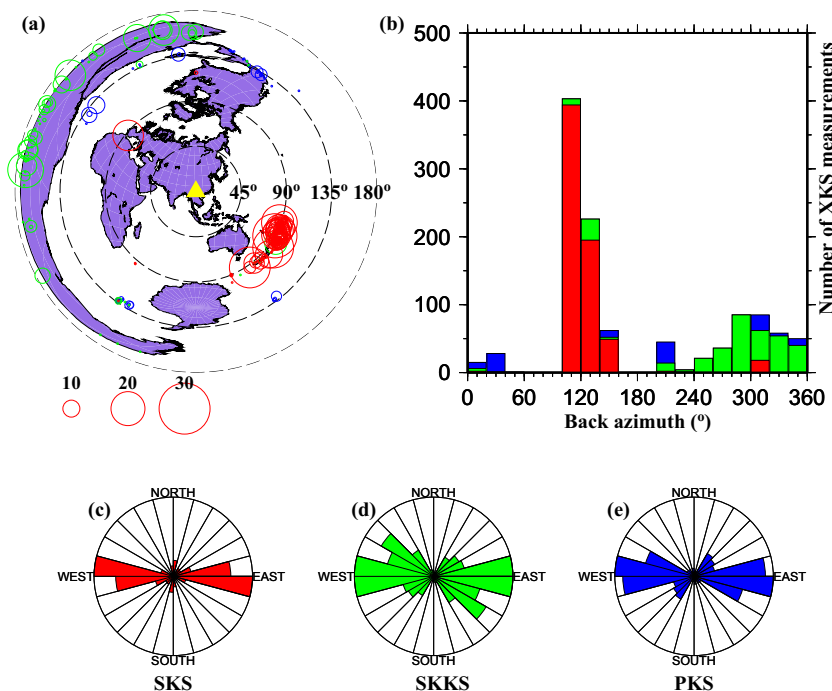


Fig. 3. (a) An azimuthal equidistant projection map centered at the study area showing earthquakes (circles) that provided one or more Quality A or B SWS measurements. The radius of the circles is proportional to the number of SWS measurements from the events. Red: SKS; green: SKKS; and blue: PKS events. (b) A histogram showing the back azimuthal distribution of the SWS measurements. (c–e) Rose diagrams illustrating the fast orientations using the SKS, SKKS, and PKS phases.

as P-to-S converted waves from the Moho, for the purpose of providing new constraints on crustal and mantle deformation associated with the continental convergence along the Himalayas, as well as the role that the subducted Indian Plate played on modulating mantle flow beneath the SE Tibetan Plateau and the northern Indochina Peninsula.

2. Data and methods

The broadband XKS seismic data set used in the study was recorded by 50 stations (Fig. 1), among which 45 were provided by the Data Management Centre of China National Seismic Network at the Institute of Geophysics, China Earthquake Administration for the recording period of 2007–2011 (Zheng et al., 2010). Data from stations MC21, MC23, MC24 (recording period: 2003–2004), KMI (1996–2017), and SLV (2008–2017) were obtained from the Incorporated Research Institutions for Seismology (IRIS) Data Management Center (DMC). The epicentral distance range for selecting the XKS events is 120° to 180° for PKS, 95° to 180° for SKKS, and 83° to 180° for SKS. The cut-off magnitude is 5.6 for events with a focal depth ≤ 100 km, and 5.5 for deeper events (Liu and Gao, 2013). Totally 291 teleseismic events that resulted in at least one well-defined SWS measurement were used in the study (Fig. 3a).

The XKS splitting parameters presented here were measured and ranked using the systematic approach of Liu and Gao (2013), which is based on the transverse energy minimization method (Silver and Chan, 1991). Previous studies show that among the several SWS measuring techniques, the transverse energy minimization approach is the most stable even when significant noise is present (Vecsey et al., 2008; Liu and Gao, 2013; Kong et al., 2015a). All the teleseismic events were band-pass filtered in the frequency band of 0.04–0.5 Hz to enhance the signal-to-noise ratio (SNR). The time window for SWS analysis was initially set as 5 s before and 20 s after the predicted XKS arrivals based on the IASP91 Earth model. An objective ranking procedure is then applied to rank the measurements as ‘A’ (good), ‘B’ (fair), ‘C’ (poor) and ‘N’ (null) based on the SNR on the original and corrected radial and transverse components (Liu et al., 2008; Liu and Gao, 2013). All the measurements were manually checked to ensure reliability, and if necessary, the time window, band-pass filtering parameters, and the rank were manually adjusted. Fig. 4 shows three measurements recorded by one of the stations, at which azimuthally dependent splitting parameters are evident.

3. Results

A total of 1119 pairs of well-defined splitting parameters with a rank of ‘A’ or ‘B’ were obtained at 50 individual stations, among which 115 are PKS, 343 are SKKS, and 661 are SKS measurements (Fig. 5). Because all stations with high quality XKS signals on the radial component have at least one A or B measurement, null measurements are not reported here as they simply reflect events with a BAZ that is similar to the fast or slow orientation (Silver and Chan, 1991; Liu and Gao, 2013).

As shown in Fig. 3, the SKS events were mostly from the western Pacific subduction zones with a BAZ range of 110° – 140° , and the SKKS events were dominantly from the western coast of South America with an epicentral distance range of 135° – 180° spanning a BAZ range of 240° – 360° . The PKS and SKKS measurements, which were excluded by most previous SWS studies, significantly improved the back azimuthal coverage, making it possible for the determination of the existence or absence of complex anisotropy which is characterized by systematic azimuthal variations of the individual splitting parameters.

3.1. Categorization of measurements based on BAZ coverage and variation

The back azimuthal variations of ϕ can be observed from the significant difference in the resulting splitting parameters obtained using

the SKS event, which are mainly from the BAZ range of 110° – 140° , and those from the SKKS events, which have a BAZ range of 240° to 360° (Fig. 6), suggesting the presence of complex anisotropy. Complex anisotropy is also unambiguously revealed by the significant difference of the observed splitting parameters from events with different back azimuths (see Fig. 4 for examples). The existence or absence of complex anisotropy can be determined based on the back azimuthal variation of the individual splitting parameters. Obviously, such a determination requires an adequate BAZ coverage.

After visual inspection of the BAZ coverage for each of the stations, we found that among the 50 stations, 22 have adequate BAZ coverage in the modulo- 90° domain, among which 7 stations show azimuthally invariant splitting parameters (Fig. 7). The splitting parameters obtained at the other 15 stations with adequate BAZ coverage are characterized by systematic back azimuthal variations with a 90° periodicity, which is consistent with the presence of a two-layered anisotropy model (Silver and Savage, 1994). Note that one of the stations (TEN), is a combination of 4 nearby stations (CZS, MZT, RHT, and XHT) in the vicinity of the Tengchong volcano. The BAZ coverage of the remaining stations is inadequate to ensure a reliable determination of the complexity of the underlain anisotropy structure. Because several studies have been conducted in the same area under the assumption of pervasive simple anisotropy (Fig. 2), those stations with an inadequate BAZ coverage are not discussed further.

3.2. Station-averaged splitting parameters

For the 7 stations with azimuthally invariant splitting parameters, which suggest the presence of simple anisotropy, station-averaged results can be adequately utilized to represent the anisotropy structure. All the stations are located at the southeastern corner of the study area and show dominantly E-W fast orientations (87° – 95°) with splitting times ranging from 0.92 to 1.2 s (Fig. 7).

3.3. Characterization of two-layered anisotropy

The upper and lower layer splitting parameters associated with a two-layered anisotropy model can be obtained by applying the grid-search technique proposed by Silver and Savage (1994), which is basically a quadruple nesting loop traversing all the candidate pairs of lower layer fast orientation (ϕ_L), lower layer splitting time (δt_L), upper layer fast orientation (ϕ_U), and upper layer splitting time (δt_U).

As demonstrated by previous complex anisotropy studies (e.g., Gao et al., 2010; Hammond et al., 2014), the resulting optimal two-layered splitting parameters are intrinsically non-unique. For instance, at station ATD located in the Afar depression, the individual splitting measurements can be fitted equally well by two different sets of parameters (Gao et al., 2010; Hammond et al., 2014). Similar to the inversion of many other types of geophysical data, in this study we take a Bayesian approach to reduce the non-uniqueness by providing additional constraints. Several different types of constraints have been applied in previous studies. The first is to fix the ϕ or δt (or both) for the upper layer as the same as the splitting parameters for the crust (e.g., Wu et al., 2015), by assuming that the upper layer anisotropy is entirely from the crust. This approach requires accurately determined crustal splitting parameters, which are not available for many of the stations in the study area. The second type of constraints assumes that the ϕ of the lower layer is the same as the absolute plate motion (APM) direction (Yang et al., 2014). This assumption might not be viable for slow-moving plates such as Eurasia and for areas with expected flow systems driven by continental collision or slab subduction, such as the study area (Wei et al., 2012). The third approach combines the splitting measurements at nearby stations, and searches for the optimal splitting parameters of the two layers (Cherie et al., 2016). Two-layered structure at individual stations are then grid-searched within given ranges of the optimal splitting parameters found using the combined data set.

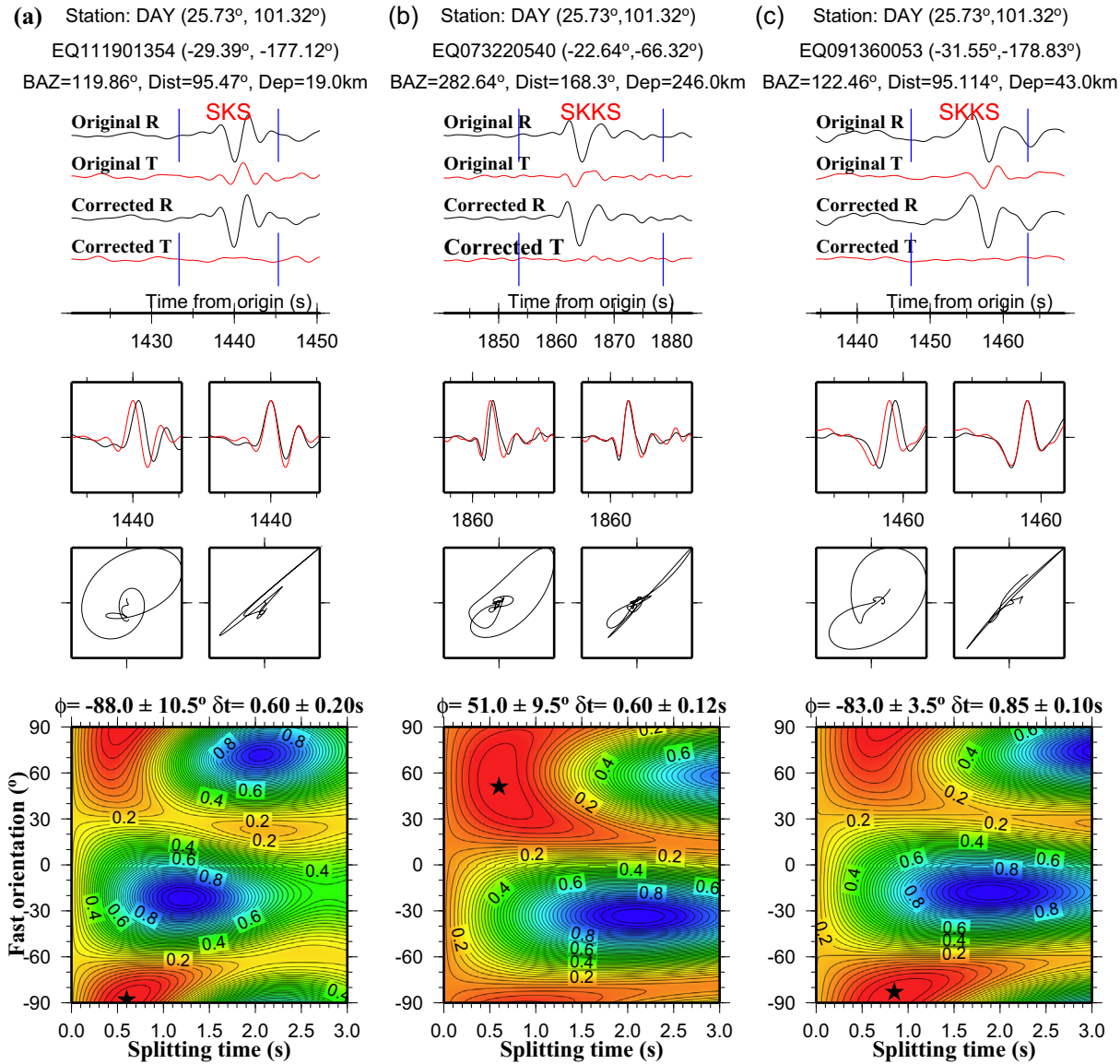


Fig. 4. Examples of SWS measurements from three events recorded by station DAY. The plots in the top row show original and corrected radial and transverse components, and plots in the central rows show the fast and slow waveforms and particle motions. The bottom plots are misfit maps, with colors representing the energy on the corrected transverse component. The optimal pair of splitting parameters correspond to the minimum value on the misfit map and are indicated by the star. Note the significant differences in the splitting parameters from the 3 events recorded by the same station.

One of the potential problems related to this approach is that ambiguities may remain in the optimal splitting parameters from the combined data set, due to the intrinsic non-uniqueness of the two-layer parameter search.

In this study we introduce another approach for providing constraints on the grid-searching of two-layered parameters. As demonstrated in the synthetic models (Fig. 8), when the δt values of the two layers are significantly different, the station-averaged fast orientation and splitting time are similar to those of the layer with the larger δt . The existence of two anisotropic layers with significantly different splitting times can be diagnosed by the following two characteristics on the variation of the individual ϕ measurements with the BAZ (in the modulo-90° domain). First, the ϕ values vary gradually within a wide BAZ range (e.g., from 12° to about 85° in Fig. 8c), and second, a large change of the ϕ values occurs in a narrow BAZ range (e.g., from 0° to 12° in Fig. 8c). The azimuthal variations of the fast orientations shown in Fig. 9 for most of the stations demonstrate the two characteristics, and thus are consistent with the existence of two layers with significantly different splitting times. Consequently, under the assumption

that the lower layer contributes more of the splitting than the upper layer, an assumption that we found is necessary to reduce the ambiguity of the resulting two layer models, we use the weighted circular mean of the fast orientations, ϕ_w , to constrain the search range of ϕ_L as ($\phi_w - 30^\circ$, $\phi_w + 30^\circ$) with an increment of 1°. The search range of δt_L is set as ($\delta t_w - 0.5$, $\delta t_w + 0.5$) with a step of 0.1 s, where δt_w is the weighted mean of the individual δt measurements. To further reduce ambiguities, in this study we assume that δt_U is no larger than half of δt_L . The weighting factor in calculating ϕ_w and δt_w is the azimuthally dependent data weighting, $1/n$, where n is the number of measurements in a 5°-wide azimuthal bin, for avoiding dominance by events from narrow BAZ bands with a relatively large number of events.

For each candidate set of two pairs of splitting parameters, a weighted misfit is computed between the observed and calculated individual splitting parameters (Gao and Liu, 2009), i.e.,

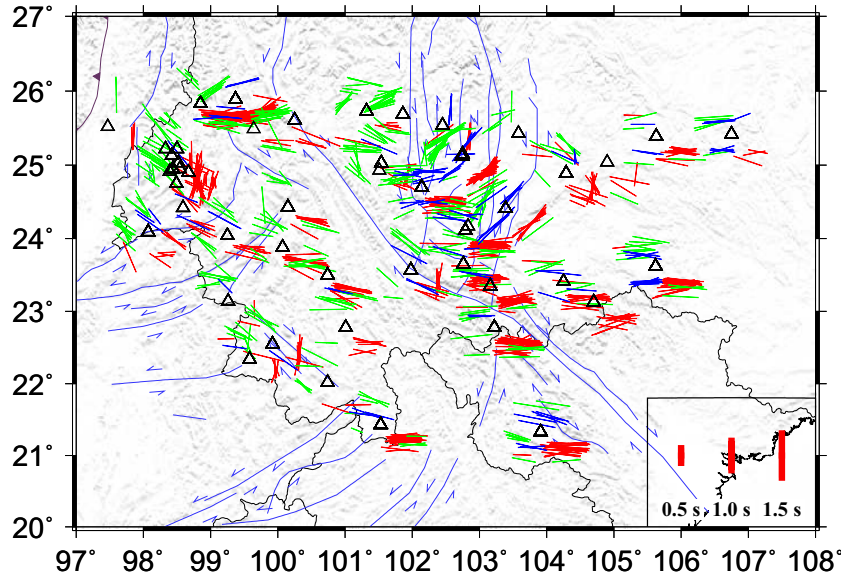


Fig. 5. Resulting Quality A and B PKs (blue bars), SKKS (green bars), and SKS (red bars) splitting parameters plotted above the ray-piercing points at 200 km depth. Blue triangles are stations.

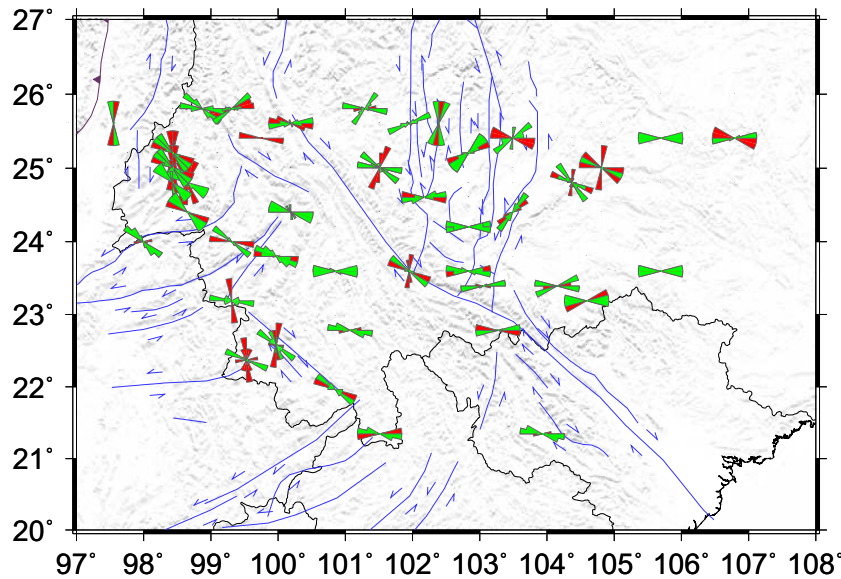


Fig. 6. Rose diagrams of fast orientations obtained using the SKS (red) and SKKS (green) phases.

$$\chi^2 = \sum_{i=1}^N \{w_1 * [\Delta_a(\phi_i^{obs}, \phi_i^{cal})/90.0] + w_2 * [|\delta t_i^{obs} - \delta t_i^{cal}|/5.0]\} * w_3(i), \quad (1)$$

where $\Delta_a(\phi_i^{obs}, \phi_i^{cal})$ represents the absolute angular difference between the observed and calculated fast orientations, N is the number of splitting parameter pairs, $w_1 = 0.5$ and $w_2 = 0.5$ are the weighting factors for the ϕ and δt measurements, respectively, and w_3 is $1/n$ that is designed to correct for the uneven azimuthal distribution of measurements.

The resulting upper and lower layer splitting parameters (Table S1) for all two-layered stations are shown in Fig. 9. The ϕ measurements of the upper layer are mostly SE-NW in the northern Shan-Thai Block, and N-S in the Yangtze Block which are consistent with the strike of major shear zones, while the lower layer is dominantly E-W (Fig. 10). The resulting two-layered anisotropic structure is in general agreement with the results from P-wave anisotropic tomography studies (Wei et al.,

2013; Wei et al., 2016), which reveal SE-NW oriented fast axis in the top 60 km, but E-W axis in the depth range of 60 to 200 km beneath the study area. Similar depth-varying anisotropy pattern is also found in surface wave tomography studies (e.g., Yao et al., 2010; Pandey et al., 2015). Relative to SWS analysis, the tomography-based results have higher vertical but poorer lateral resolution.

4. Discussion

4.1. Upper layer anisotropy and crustal contribution

Mineral physics experiments show that mica-or-amphibole-bearing metamorphic rocks collected from the study area are significantly anisotropic, and are suggested to be the source of crustal anisotropy with anomalously large splitting times of up to 1.3 s (Ji et al., 2015; Kong et al., 2016). In order to characterize crustal anisotropy and isolate mantle contributions to the results from XKS splitting, crustal

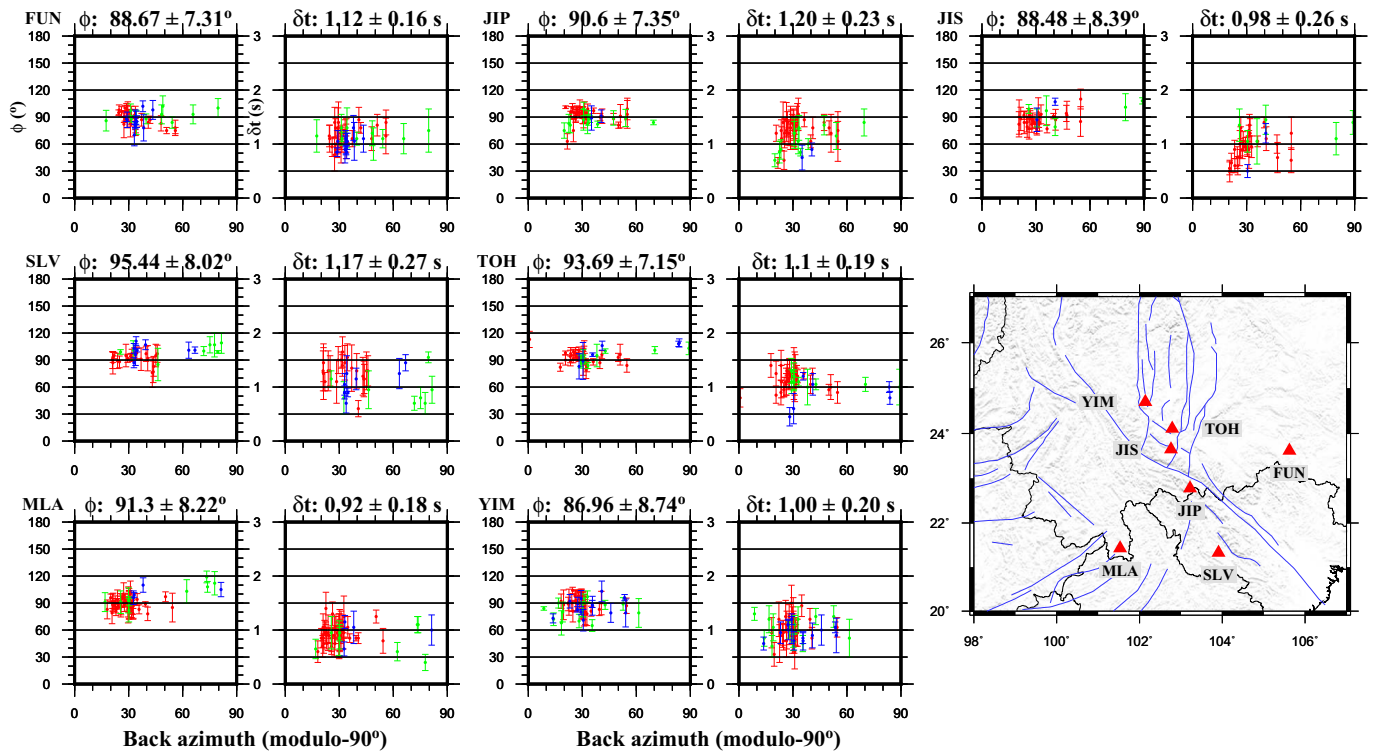


Fig. 7. SWS measurements from azimuthally invariant stations plotted against modulo-90° back azimuth. The inset at the lower-right corner shows the distribution of the 7 stations.

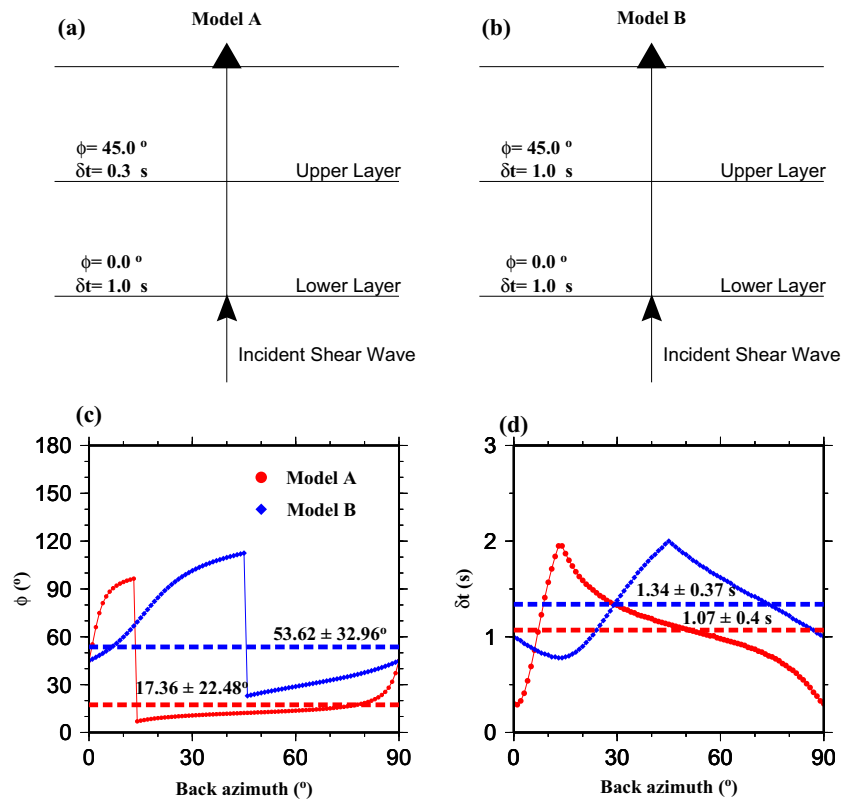


Fig. 8. Two models of two-layered anisotropy and resulting theoretical splitting parameters. (a) Model A. (b) Model B. (c) Fast orientations obtained using Silver and Savage (1994) for Model A (red) and B (blue). (d) Same as (c) but for splitting times. The dashed lines are station averaged splitting parameters.

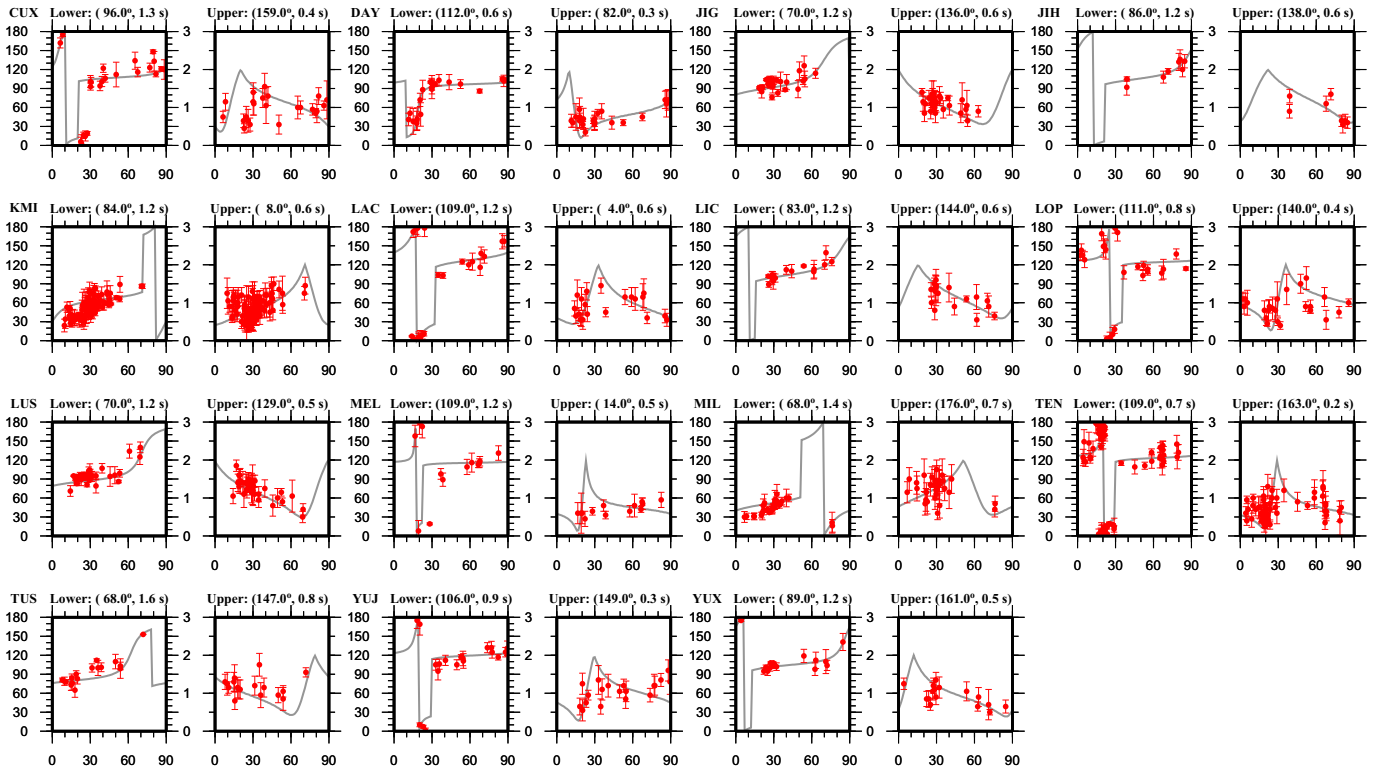


Fig. 9. Azimuthal variations of splitting parameters for 15 two-layered stations. The gray lines are the predicted splitting parameters calculated using the optimal splitting parameters for the two layers and an uniform frequency of 0.25 Hz.

anisotropy parameters are computed based on the sinusoidal moveout of P-to-S conversions from the Moho (Fig. 11) (Rumpker et al., 2014), a technique that has been applied to investigate crustal anisotropic structures in the eastern Tibetan Plateau and adjacent areas (Kong et al., 2016) and elsewhere. In this study, teleseismic events with a BAZ in the range of 0–180°, which contains the vast majority of the radial receiver functions, are utilized to compute crustal anisotropy

parameters. Data selection and processing procedure and criteria are identical to those used by Kong et al. (2016). A total of 15 crustal anisotropy measurements are obtained (Fig. 10 and Table S2) including one null measurement ($\delta t < 0.1$ s) observed at station SLV. The crustal anisotropy measurements are in general agreement with those obtained by Chen et al. (2013), Sun et al. (2012), and Cai et al. (2016), except that the δt values in this study are mostly larger than those in Chen et al.

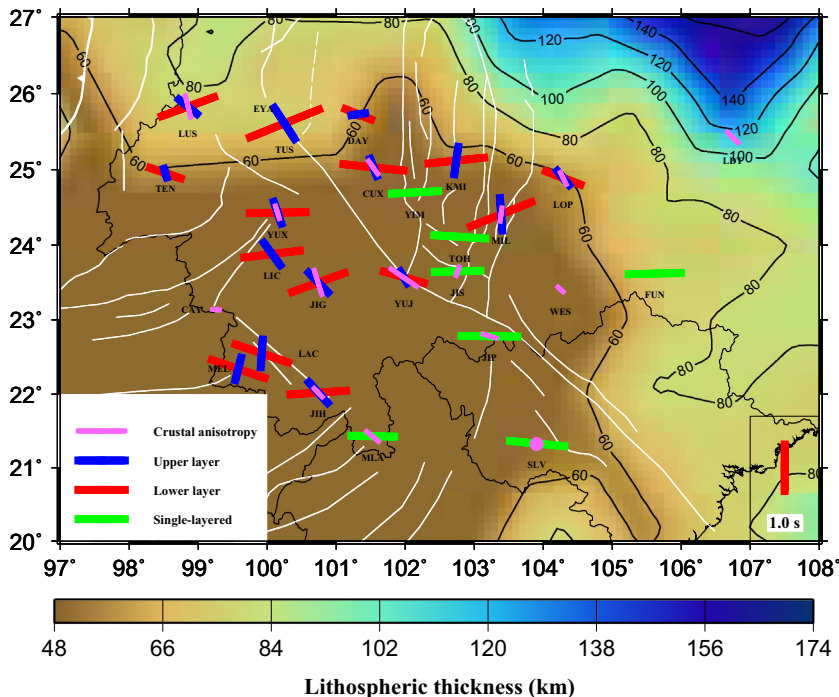


Fig. 10. Resulting splitting parameters for all two-layered stations (red bars: lower layer; blue bars: upper layer), station-averaged splitting parameters for single-layered stations (green bars), and the crustal anisotropy measurements (pink bars). The pink dot indicates null crustal anisotropy. The background color and contour lines represent the lithospheric thickness (Pasyanos et al., 2014).

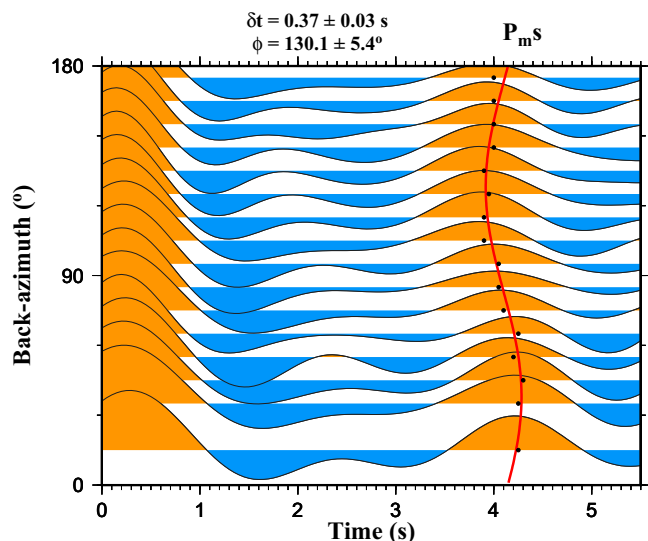


Fig. 11. Azimuthal-band-averaged radial receiver functions recorded by station MLA plotted against the BAZ. The black dots represent the peak of the P-to-S conversions from the Moho, and the red line is the best fitting curve computed based on Eq. 1 in Kong et al. (2016) using the optimal pair of the splitting parameters.

(2013). They are also similar to the fast orientations inferred from the Love-Rayleigh phase speed difference (Xie et al., 2017). The smaller δt values might be partially attributed to the application of the multiple-event stacking technique used by some of the previous studies, which may underestimate the δt (Kong et al., 2015b).

The resulting fast orientations of crustal anisotropy are mostly consistent with the upper layer ϕ from XKS splitting (Fig. 10), and the crustal δt values are comparable to the upper layer δt . Comparison using 8 stations that have both upper layer and crustal anisotropy measurements shows that the averaged differences of ϕ and δt are 16.4° and 0.06 s, respectively. Such consistencies suggest that the observed upper layer anisotropy is mostly from the crust and can be attributed to crustal fabrics deformed by compressional folding and shear (Ji et al., 2015; Kong et al., 2016).

4.2. Anisotropy induced by mantle flow

The majority of the study area is characterized by a thin lithosphere with a thickness of 60–100 km (Fig. 10; (Pasyanos et al., 2014)) and a Moho depth of 40–70 km (Sun et al., 2012). The fast orientations of the lower layer and single-layered anisotropy are inconsistent with the strikes of the major shear zones that are mostly SE–NW (e.g., the Red River Fault) or SSW–NNE (e.g., the Xianshuihe–Xiaojiang Fault Zone). The small thickness of the mantle lithosphere and the inconsistencies between the fast orientations and the strike directions suggest that the lower layer and single-layered anisotropy are mainly in the asthenosphere, or the rheologically transitional layer between the lithosphere and asthenosphere (e.g., Reed et al., 2017; Yang et al., 2017).

As shown in Figs. 5 and 10, the fast orientations of the lower layer and those from the 7 single-layered stations are dominantly E–W, which differs by 15–20° from the fast orientations predicted based on the HS3-NUVEL-1A (Gripp and Gordon, 2002) and NNR-MORVEL56 (Argus et al., 2011) APM models. In the study area, the plate motion rate for both models (22–24 mm/yr) is lower than the threshold value of 30 mm/yr, below which the APM has insignificant influence on seismic azimuthal anisotropy (Debayle and Ricard, 2013). In addition, even if APM is a major contributor to the observed anisotropy in most areas of East Asia, the presence of a slab (Wei et al., 2012) may modulate the flow system and result in a complicated flow pattern which is not observed in the study area. Therefore, while the possibility that the

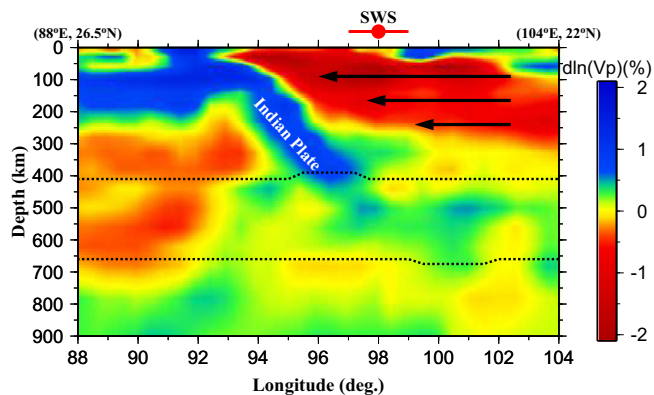


Fig. 12. P-wave relative velocity anomalies across a WNW-ESE oriented profile traversing the study area generated based on the results of Wei et al. (2012). The arrows represent slab rollback induced flow system, and the two dashed horizontal lines are the 410 and 660 km discontinuities. The red bar denotes the observed anisotropy. The coordinates shown at the top show the approximate locations of the two ends of the profile.

observed anisotropy primarily originates from the APM cannot be completely ruled out, we postulate that APM may not be the dominating process.

Recent focal mechanism and tomography studies (Fig. 12; Wei et al., 2012) suggest that the eastward subduction of the Indian Plate is probably inactive (Rao and Kumar, 1999; Kundu and Gahalaut, 2012) and is undergoing slab retreat (Li et al., 2008). If this is true, the fast orientations of the lower layer and single-layered anisotropy can be adequately explained by a mantle flow system moving toward the trench induced by the westward retreat and rollback of the subducted Indian Plate along the Burmese arc (Fig. 12). Such a mechanism has recently been invoked to explain the mostly E–W fast orientations observed on the Indochina Peninsula (Yu et al., 2018) and is suggested by geodynamic modeling (Sternai et al., 2014).

5. Conclusions

This first systematic investigation of complex azimuthal anisotropy beneath the transitional region between the SE Tibetan Plateau and the Indochina Peninsula reveals spatially widespread existence of a two-layered anisotropy structure. The splitting parameters for the upper layer are comparable to those obtained for the crust, and can thus be attributed to rock fabrics with vertical foliation planes created by crustal compression and shearing. The lower layer of anisotropy as well as the simple anisotropic structure beneath the stations with azimuthally invariant splitting parameters are most likely from simple shear in the upper asthenosphere. The observed mantle anisotropy is consistent with a flow system induced by the westward rollback of the subducted Indian Plate.

Acknowledgments

We thank the Data Management Centre of China National Seismic Network at Institute of Geophysics, China Earthquake Administration (SEISDMC, doi:10.7914/SN/CB) and the IRIS DMC for providing the seismic data. W. Wei provided their tomographic data that we used to produce (Fig. 12). Comments from two anonymous reviewers improved the manuscript. The study was partially supported by grant no. HYGG1802 of the Scientific Research Fund of the Second Institute of Oceanography State Oceanic Administration of China to F.K., and the United States National Science Foundation grants EAR-0911346, EAR-1321656, and EAR-1830644 to K.L. and S.G.

Appendix A. Supplementary data

Supplementary data to this article can be found online at <https://doi.org/10.1016/j.tecto.2018.09.013>.

References

- Argus, D.F., Gordon, R.G., DeMets, C., 2011. Geologically current motion of 56 plates relative to the no-net-rotation reference frame. *Geochem. Geophys. Geosyst.* 12, Q11001. <https://doi.org/10.1029/2011GC003751>.
- Ben Ismail, W., Mainprice, D., 1998. An olivine fabric database: an overview of upper mantle fabrics and seismic anisotropy. *Tectonophysics* 296, 145–157. [https://doi.org/10.1016/S0040-1951\(98\)00141-3](https://doi.org/10.1016/S0040-1951(98)00141-3).
- Bird, P., 1991. Lateral extrusion of lower crust from under high topography in the isostatic limit. *J. Geophys. Res.* 96, 10275–10286. <https://doi.org/10.1029/91JB00370>.
- Cai, Y., Wu, J., Fang, L., Wang, W., Yi, S., 2016. Crustal anisotropy and deformation of the southeastern margin of the Tibetan Plateau revealed by Pms splitting. *J. Asian Earth Sci.* 121, 120–126. <https://doi.org/10.1016/j.jseas.2016.02.005>.
- Chang, L., Wang, C., Ding, Z., 2006. A study on SKS splitting beneath the Yunnan region, southwestern China. *Chin. J. Geophys.* 49, 167–175. <https://doi.org/10.1002/cjg2.824>.
- Chen, L., Capitanio, F.A., Liu, L., Gerya, T.V., 2017. Crustal rheology controls on the Tibetan plateau formation during India-Asia convergence. *Nat. Commun.* 8, 15992. <https://doi.org/10.1038/ncomms15992>.
- Chen, Y., Zhang, Z., Sun, C., Badal, J., 2013. Crustal anisotropy from Moho converted Ps wave splitting analysis and geodynamic implications beneath the eastern margin of Tibet and surrounding regions. *Gondwana Res.* 24, 946–957. <https://doi.org/10.1016/j.gr.2012.04.003>.
- Cherie, S.G., Gao, S.S., Liu, K.H., Elsheikh, A.A., Kong, F., Reed, C.A., Yang, B.B., 2016. Shear wave splitting analyses in Tian Shan: geodynamic implications of complex seismic anisotropy. *Geochem. Geophys. Geosys.* 17, 1975–1989. <https://doi.org/10.1002/2016GC006269>.
- Debayle, E., Ricard, Y., 2013. Seismic observations of large-scale deformation at the bottom of fast-moving plates. *Earth Planet. Sci. Lett.* 376, 165–177. <https://doi.org/10.1016/j.epsl.2013.06.025>.
- England, P., Houseman, G., 1986. Finite strain calculations of continental deformation: 2. comparison with the India-Asia collision zone. *J. Geophys. Res.* 91, 3664–3676. <https://doi.org/10.1029/JB091iB03p03664>.
- England, P., Molnar, P., 1990. Right-lateral shear and rotation as the explanation for strike-slip faulting in east Tibet. *Nature* 344, 140–142.
- Flesch, L.M., Holt, W.E., Silver, P.G., Stephenson, M., Wang, C., Chan, W.W., 2005. Constraining the extent of crust-mantle coupling in central Asia using GPS, geologic, and shear wave splitting data. *Earth Planet. Sci. Lett.* 238, 248–268. <https://doi.org/10.1016/j.epsl.2005.06.023>.
- Gan, W., Zhang, P., Shen, Z., Niu, Z., Wang, M., Wan, Y., Zhou, D., Cheng, J., 2007. Present-day crustal motion within the Tibetan Plateau inferred from GPS measurements. *J. Geophys. Res.* 112, B08416. <https://doi.org/10.1029/2005JB004120>.
- Gao, S., Davis, P.M., Liu, H., Slack, P.D., Zorin, Y.u.A., Mordvinova, V.V., Kozhevnikov, V.M., Meyer, R.P., 1994. Seismic anisotropy and mantle flow beneath the Baikal rift zone. *Nature* 371, 149–151. <https://doi.org/10.1038/371149a0>.
- Gao, S.S., Liu, K.H., 2009. Significant seismic anisotropy beneath the southern Lhasa Terrane, Tibetan Plateau. *Geochem. Geophys. Geosys.* 10, Q02008. <https://doi.org/10.1029/2008GC002227>.
- Gao, S.S., Liu, K.H., Abdelsalam, M.G., 2010. Seismic anisotropy beneath the Afar Depression and adjacent areas: implications for mantle flow. *J. Geophys. Res.* 115, B12330. <https://doi.org/10.1029/2009JB007141>.
- Gripp, A.E., Gordon, R.G., 2002. Young tracks of hotspots and current plate velocities. *Geophys. J. Int.* 150, 321–361. <https://doi.org/10.1046/j.1365-246X.2002.01627.x>.
- Hammond, J.O.S., Kendall, J.M., Wokey, J., Stuart, G.W., Keir, D., Ayele, A., 2014. Differentiating flow, melt, or fossil seismic anisotropy beneath Ethiopia. *Geochem. Geophys. Geosyst.* 15, 1878–1894. <https://doi.org/10.1002/2013GC005185>.
- Huang, Z., Wang, P., Xu, M., Wang, L., Ding, Z., Wu, Y., Xu, M., Mi, N., Yu, D., Li, H., 2015a. Mantle structure and dynamics beneath SE Tibet revealed by new seismic images. *Earth Planet. Sci. Lett.* 411, 100–111. <https://doi.org/10.1016/j.epsl.2014.11.040>.
- Huang, Z., Wang, L., Xu, M., Ding, Z., Wu, Y., Wang, P., Mi, N., Yu, D., Li, H., 2015b. Teleseismic shear-wave splitting in SE Tibet: insight into complex crust and upper-mantle deformation. *Earth Planet. Sci. Lett.* 432, 354–362. <https://doi.org/10.1016/j.epsl.2015.10.027>.
- Huang, Z., Zhao, D., Wang, L., 2015c. P wave tomography and anisotropy beneath Southeast Asia: insight into mantle dynamics. *J. Geophys. Res.* 120, 5154–5174. <https://doi.org/10.1002/2015JB012098>.
- Ji, S., Shao, T., Michibayashi, K., Oya, S., Satsukawa, T., Wang, Q., Zhao, W., Salisbury, M.H., 2015. Magnitude and symmetry of seismic anisotropy in mica- and amphibole-bearing metamorphic rocks and implications for tectonic interpretation of seismic data from the southeast Tibetan Plateau. *J. Geophys. Res.* 120, 6404–6430. <https://doi.org/10.1002/2015JB012209>.
- Kong, F., Gao, S.S., Liu, K.H., 2015a. A systematic comparison of the transverse energy minimization and splitting intensity techniques for measuring shear-wave splitting parameters. *Bull. Seismol. Soc. Am.* 105, 230–239. <https://doi.org/10.1785/0120140108>.
- Kong, F., Gao, S.S., Liu, K.H., 2015b. Applicability of the multiple-event stacking technique for shear-wave splitting analysis. *Bull. Seismol. Soc. Am.* 105, 3156–3166. <https://doi.org/10.1785/0120150078>.
- Kong, F., Wu, J., Liu, K.H., Gao, S.S., 2016. Crustal anisotropy and ductile flow beneath the eastern Tibetan Plateau and adjacent areas. *Earth Planet. Sci. Lett.* 422, 72–79. <https://doi.org/10.1016/j.epsl.2016.03.003>.
- Kundu, B., Gahalaut, V.K., 2012. Earthquake occurrence processes in the Indo-Burmese wedge and Sagaing fault region. *Tectonophysics* 524, 135–146. <https://doi.org/10.1016/j.tecto.2011.12.031>.
- Lei, J., Zhao, D., Su, Y., 2009. Insight into the origin of the Tengchong intraplate volcano and seismotectonics in southwest China from local and teleseismic data. *J. Geophys. Res.* 114, B05302. <https://doi.org/10.1029/2008JB005881>.
- Lev, E., Long, M.D., van der Hilst, R.D., 2006. Seismic anisotropy in Eastern Tibet from shear wave splitting reveals changes in lithospheric deformation. *Earth Planet. Sci. Lett.* 251, 293–304. <https://doi.org/10.1016/j.epsl.2006.09.018>.
- Li, C., van der Hilst, R.D., Meltzer, A.S., Engdahl, E.R., 2008. Subduction of the Indian lithosphere beneath the Tibetan Plateau and Burma. *Earth Planet. Sci. Lett.* 274, 157–168. <https://doi.org/10.1016/j.epsl.2008.07.016>.
- Liu, K.H., Gao, S.S., 2013. Making reliable shear-wave splitting measurements. *Bull. Seismol. Soc. Am.* 103, 2680–2693. <https://doi.org/10.1785/0120120355>.
- Liu, K.H., Gao, S.S., Gao, Y., Wu, J., 2008. Shear wave splitting and mantle flow associated with the deflected Pacific slab beneath northeast Asia. *J. Geophys. Res.* 113, B01305. <https://doi.org/10.1029/2007JB005178>.
- Liu, M., Cui, X., Liu, F., 2004. Cenozoic rifting and volcanism in eastern China: a mantle dynamic link to the Indo-Asian collision? *Tectonophysics* 393, 29–42. <https://doi.org/10.1016/j.tecto.2004.07.029>.
- Pandey, S., Yuan, X., Debayle, E., Tilmann, F., Priestley, K., Li, X., 2015. Depth-variant azimuthal anisotropy in Tibet revealed by surface wave tomography. *Geophys. Res. Lett.* 42, 4326–4334. <https://doi.org/10.1002/2015GL063921>.
- Pasyanos, M.E., Masters, T.G., Laske, G., Ma, Z., 2014. LITHO1.0: an updated crust and lithospheric model of the Earth. *J. Geophys. Res.* 119, 2153–2173. <https://doi.org/10.1002/2013JB010626>.
- Rao, N.P., Kumar, M.R., 1999. Evidences for cessation of Indian plate subduction in the Burmese arc region. *Geophys. Res. Lett.* 26, 3149–3152. <https://doi.org/10.1029/1999GL005396>.
- Reed, C.A., Liu, K.H., Yu, Y., Gao, S.S., 2017. Seismic anisotropy and mantle dynamics beneath the Malawi Rift zone, East Africa. *Tectonics* 36, 1338–1351. <https://doi.org/10.1002/2017TC004519>.
- Royden, L.H., Burchfiel, B.C., King, R.W., Wang, E., Chen, Z., Shen, F., Liu, Y., 1997. Surface deformation and lower crustal flow in eastern Tibet. *Science* 276, 788–790. <https://doi.org/10.1126/science.276.5313.788>.
- Rumpker, G., Kaviani, A., Latifi, K., 2014. Ps-splitting analysis for multilayered anisotropic media by azimuthal stacking and layer stripping. *Geophys. J. Int.* 199, 146–163. <https://doi.org/10.1093/gji/ggu154>.
- Searle, M.P., 2006. Role of the Red River Shear Zone, Yunnan and Vietnam, in the continental extrusion of SE Asia. *J. Geol. Soc.* 163, 1025–1036. <https://doi.org/10.1144/0016-76492005-144>.
- Searle, M.P., Elliott, J.R., Phillips, R.J., Chung, S.L., 2011. Crustal-lithospheric structure and continental extrusion of Tibet. *J. Geol. Soc.* 168, 633–672. <https://doi.org/10.1144/0016-76492010-139>.
- Shi, Y., Gao, Y., Su, Y., Wang, Q., 2012. Shear-wave splitting beneath Yunnan area of Southwest China. *Earth Sci.* 25, 25–34. <https://doi.org/10.1007/s11589-012-0828-4>.
- Silver, P.G., Savage, M.K., 1994. The interpretation of shear-wave splitting parameters in the presence of two anisotropic layers. *Geophys. J. Int.* 119, 949–963. <https://doi.org/10.1111/j.1365-246X.1994.tb04027.x>.
- Silver, P.G., Chan, W.W., 1991. Shear wave splitting and subcontinental mantle deformation. *J. Geophys. Res.* 96, 16429–16454. <https://doi.org/10.1029/91JB00899>.
- Sol, S., Meltzer, A., Burgmann, R., van der Hilst, R.D., King, R., Chen, Z., Koons, P.O., Lev, E., Liu, Y.P., Zeitler, P.K., Zhang, X., Zhang, J., Zurek, B., 2007. Geodynamics of the southeastern Tibetan Plateau from seismic anisotropy and geodesy. *Geology* 35, 563–566. <https://doi.org/10.1130/G23408A1>.
- Sternai, P., Jolivet, L., Menant, A., Gerya, T., 2014. Driving the upper plate surface deformation by slab rollback and mantle flow. *Earth Planet. Sci. Lett.* 405, 110–118. <https://doi.org/10.1016/j.epsl.2014.08.023>.
- Styron, R., Taylor, M., Okoronkwo, K., 2010. Database of active structures from the Indo-Asian collision. *Eos. Trans. AGU* 91, 181–182. <https://doi.org/10.1029/2010EO200001>.
- Sun, Y., Niu, F., Liu, H., Chen, Y., Liu, J., 2012. Crustal structure and deformation of the SE Tibetan plateau revealed by receiver function data. *Earth Planet. Sci. Lett.* 349–350, 186–197. <https://doi.org/10.1016/j.epsl.2012.07.007>.
- Tapponnier, P., 1982. Propagating extrusion tectonics in asia: new insights from simple experiments with plasticine. *Geology* 10, 611–616. [https://doi.org/10.1130/0091-7613\(1982\)10<611:PETIAN>2.0.CO;2](https://doi.org/10.1130/0091-7613(1982)10<611:PETIAN>2.0.CO;2).
- Vecsey, L., Plomerova, J., Babuska, V., 2008. Shear-wave splitting measurements-problems and solutions. *Tectonophysics* 462, 178–196. <https://doi.org/10.1016/j.tecto.2008.01.021>.
- Wang, C., Flesch, L.M., Chang, L., Zheng, T., 2013. Evidence of active mantle flow beneath South China. *Geophys. Res. Lett.* 40, 5137–5141. <https://doi.org/10.1002/grl.50987>.
- Wang, C., Flesch, L.M., Silver, P.G., Chang, L., Chan, W.W., 2008. Evidence for mechanically coupled lithosphere in central Asia and resulting implications. *Geology* 36, 363–366. <https://doi.org/10.1130/G24450A1>.
- Wang, Z., Zhao, D., Wang, J., 2010. Deep structure and seismogenesis of the north-south seismic zone in southwest China. *J. Geophys. Res.* 115, B12334. <https://doi.org/10.1029/2010JB007797>.
- Wei, W., Xu, J., Zhao, D., Shi, Y., 2012. East Asia mantle tomography: new insight into plate subduction and intraplate volcanism. *J. Asian Earth Sci.* 60, 88–103. <https://doi.org/10.1016/j.jseas.2012.08.001>.
- Wei, W., Zhao, D., Xu, J., 2013. P-wave anisotropic tomography in Southeast Tibet: new

- insight into the lower crustal flow and seismotectonics. *Phys. Earth Planet. Inter.* 222, 47–57. <https://doi.org/10.1016/j.pepi.2013.07.002>.
- Wei, W., Zhao, D., Xu, J., Zhou, B., Shi, Y., 2016. Depth variations of P-wave azimuthal anisotropy beneath mainland China. *Sci. Rep.* 6, 29614. <https://doi.org/10.1038/srep29614>.
- Wu, J., Zhang, Z., Kong, F., Yang, B.B., Yu, Y., Liu, K.H., Gao, S.S., 2015. Complex seismic anisotropy beneath western Tibet and its geodynamic implications. *Earth Planet. Sci. Lett.* 413, 167–175. <https://doi.org/10.1016/j.epsl.2015.01.002>.
- Xie, J., Ritzwoller, M.H., Shen, W., Wang, W., 2017. Crustal anisotropy across eastern Tibet and surroundings modeled as a depth-dependent tilted hexagonally symmetric medium. *Geophys. J. Int.* 209, 466–491. <https://doi.org/10.1093/gji/ggx004>.
- Yang, B.B., Gao, S.S., Liu, K.H., Elsheikh, A.A., Lemnifi, A.A., Refayee, H.A., Yu, Y., 2014. Seismic anisotropy and mantle flow beneath the northern Great Plains of North America. *J. Geophys. Res.* 119, 1971–1985. <https://doi.org/10.1002/2013JB010561>.
- Yang, B.B., Liu, Y., Dahm, H., Liu, K.H., Gao, S.S., 2017. Seismic azimuthal anisotropy beneath the eastern United States and its geodynamic implications. *Geophys. Res. Lett.* 44, 2670–2678. <https://doi.org/10.1002/2016GL071227>.
- Yao, H., van der Hilst, R.D., Montagner, J.P., 2010. Heterogeneity and anisotropy of the lithosphere of SE Tibet from surface wave array tomography. *J. Geophys. Res.* 115, B12307. <https://doi.org/10.1029/2009JB007142>.
- Yin, A., Harrison, T.M., 2000. Geologic evolution of the Himalayan-Tibetan orogen. *Annu. Rev. Earth Planet. Sci.* 28, 211–280. <https://doi.org/10.1146/annurev.earth.28.1.211>.
- Yu, Y., Gao, S.S., Liu, K.H., Yang, T., Xue, M., Le, K.P., Gao, J., 2018. Characteristics of the mantle flow system beneath the indochina peninsula revealed by teleseismic shear wave splitting analysis. *Geochem. Geophys. Geosys.* <https://doi.org/10.1029/2018GC007474>.
- Zhang, S., Karato, S., 1995. Lattice preferred orientation of olivine aggregates deformed in simple shear. *Nature* 375, 774–777. <https://doi.org/10.1038/375774a0>.
- Zhang, Z., Yuan, X., Chen, Y., Tian, X., Kind, R., Li, X., Teng, J., 2010. Seismic signature of the collision between the east Tibetan escape flow and the Sichuan Basin. *Earth Planet. Sci. Lett.* 292, 254–264. <https://doi.org/10.1016/j.epsl.2010.01.046>.
- Zhao, L., Luo, Y., Liu, T., Luo, Y., 2013a. Earthquake focal mechanisms in Yunnan and their inference on the regional stress field. *Bull. Seismo. Soc. Am.* 103, 2498–2507. <https://doi.org/10.1785/0120120309>.
- Zhao, L., Zheng, T., Lu, G., 2013b. Distinct upper mantle deformation of cratons in response to subduction: constraints from SKS wave splitting measurements in eastern China. *Gondwana Res.* 23, 39–53. <https://doi.org/10.1016/j.gr.2012.04.007>.
- Zheng, X., Yao, Z., Liang, J., Zheng, J., 2010. The role played and opportunities provided by IGP DMC of China National Seismic Network in Wenchuan earthquake disaster relief and researches. *Bull. Seismo. Soc. Am.* 100, 2866–2872. <https://doi.org/10.1785/0120090257>.